Nanoscale

PAPER

View Article Online
View Journal | View Issue

Cite this: *Nanoscale*, 2024, **16**, 3729

Simple hybrid polymeric nanostructures encapsulating macro-cyclic Gd/Eu based complexes: luminescence properties and application as MRI contrast agent†

Marjorie Yon,[a] Lucie Esmangard,[a] Morgane Enel,[b] Franck Desmoulin,[c,d] Carine Pestourie,[d] Nadine Leygue,[b] Christophe Mingotaud,[a] Chantal Galaup *[b] and Jean-Daniel Marty *[a]

Received 2nd December 2023,
Accepted 23rd January 2024

DOI: 10.1039/d3nr06162k

rsc.li/nanoscale

Lanthanide-based macrocycles are successfully incorporated into hybrid polyionic complexes, formed by adding a mixture of zirconium ions to a solution of a double-hydrophilic block copolymer. The resulting nanoobjects with an average radius of approximately 10–15 nm present good colloidal and chemical stability in physiological media even in the presence of competing ions such as phosphate or calcium ions. The final optical and magnetic properties of these objects benefit from both their colloidal nature and the specific properties of the complexes. Hence these new nanocarriers exhibit enhanced T1 MRI contrast, when administered intravenously to mice.

1. Introduction

Magnetic resonance imaging (MRI) is a powerful medical diagnostic tool, the efficiency of which is significantly enhanced by the use of exogeneous contrast agents (CAs). Among these, CAs based on the gadolinium ions with seven unpaired electrons, paramagnetic properties and a high magnetic moment are most commonly employed as T_1 or positive contrast agents. To mitigate their cytotoxicity,[1–3] gadolinium ions are generally chelated with linear (MAGNEVIST®,[4] OMNISCAN®,[5,6] OPTIMARK® and MultiHance®[7]) or macrocycle multifunctional ligands (PROHANCE®, DOTAREM®, GADOVIST®).[8] However, molecular complexes possess limitations, such as residual toxicity and reduced efficiency at the higher magnetic fields of modern MRI instruments.[5,9,10] Consequently, in 2017 European medicine agency suspended the authorization of the intravenous linear Gd-based CAs. Therefore, there is an ongoing need for new CAs with enhanced properties such as extended circulation lifetime or higher relaxivity.[11]

The immobilization of Gd-chelates onto macromolecules or nano-objects is one approach to provide more efficient CAs.[12–14] Indeed, Gd ions located within the colloidal species will rotate at the same low rate as the entire nanoparticles (NPs), thereby increasing the observed relaxivity r_1 (the longitudinal relaxation rate $1/T_1$ normalized by the concentration of CAs). An alternative involves inducing the formation of aggregates through the complexation of negatively charged Gd complexes with a diblock cationic copolymer bearing simple functional groups.[15] Another option is to use hybrid polyion complexes (HPICs) formed by the complexation of free gadolinium ions with diblock copolymers functionalized with lanthanide-chelate groups that interact[16,17] or more simple function. Hence, poly (ethylene oxide) (PEO) double hydrophilic block copolymer comprising a complexing block based on poly(acrylic acid) (PAA) or poly(vinyl phosphonic acid) (PVPA) exhibit exceptionally high stability upon dilution. These colloids, having a mean radius *ca.* 10 nm, generate high water proton relaxivities *in vitro* and an excellent tolerance *in vivo* after intravenous injection into a rat model, resulting positive signal enhancement.[18–20] Combining different ions within the same HPIC is also a promising strategy for obtaining multifunctional systems with enhanced functions.[21–24] Hence, the insertion of zirconyl ions, reported to be without adverse effects,[25] in addition to gadolinium ions led to the formation of Gd/Zr@HPICs with enhanced stability due to strong affinity of zirconium ions for carboxylate function and improved relaxation properties.[26]

[a]*Laboratoire Softmat, University of Toulouse, CNRS UMR 5623, University Toulouse III – Paul Sabatier, France, 118, route de Narbonne, 31062 Toulouse Cedex 9, France. E-mail: jean-daniel.marty@univ-tlse3.fr*
[b]*Laboratoire SPCMIB, CNRS UMR 5068, University of Toulouse, University Toulouse III - Paul Sabatier 118, route de Narbonne 31062, Toulouse Cedex 9, France. E-mail: chantal.galaup@univ-tlse3.fr*
[c]*Toulouse NeuroImaging Center (ToNIC), Inserm, University of Toulouse - Paul Sabatier, Toulouse, France*
[d]*CREFRE-Anexplo, University of Toulouse, Inserm, UT3, ENVT, Toulouse, France*

†Electronic supplementary information (ESI) available: Synthesis of complexing ligand and additional data for the characterization of materials. See DOI: https://doi.org/10.1039/d3nr06162k

In this article, we will present a strategy that combines the use of macrocyclic complexes and HPICs. This approach avoids the tedious grafting protocol on the polymer structure. The insertion of europium(III) and gadolinium(III), lanthanide chelates within HPICs structures is ensured, as illustrated in Scheme 1 (right), through the simple mixing of a specifically designed chelate, zirconyl ions and PEO_{6k}-*b*-PAA_{3k} copolymer. This strategy will be compared to the one using lanthanide ions in their free form (Scheme 1, left).

The 12-membered tetraazamacrocyclic chelate PCTA-COOH (PCTA: 3,6,9,15-tetraaz-abicyclo[9.3.1]pentadeca-1(15),11,13-triene-3,6,9-triacetic acid) investigated in this work for the incorporation of Eu^{3+} or Gd^{3+} ions is a heptadentate ligand derived from PCTA ligand. PCTA is known as a versatile chelate able of complexing various M^{2+} and M^{3+} ions for biomedical applications such as diagnostic and radiotherapeutic (Fig. 1). In the field of magnetic resonance imaging (MRI), PCTA forms very stable Gd^{3+} complex ($\log K_{GdL} = 20.39$) with a kinetic inertness favorable for *in vivo* applications.[27] Due to the presence of two water molecules in the first coordination sphere of the metal, the Gd-PCTA complex displays a higher water relaxivity (r_1 = 5.4 s^{-1} mM^{-1} at 20 MHz and 37 °C) than the clinical Gd contrast agent DOTAREM® or the monoaqua $[Gd\text{-}DOTA]^-$ complex (r_1 = 3.5 s^{-1} mM^{-1} at 20 MHz and 37 °C) (Fig. 1). This characteristic makes it a promising candidate as an MRI contrast agent.[28–30] The PCTA-COOH chelate contains a pyridine functionalized at the 4-position by a carboxylic acid function,

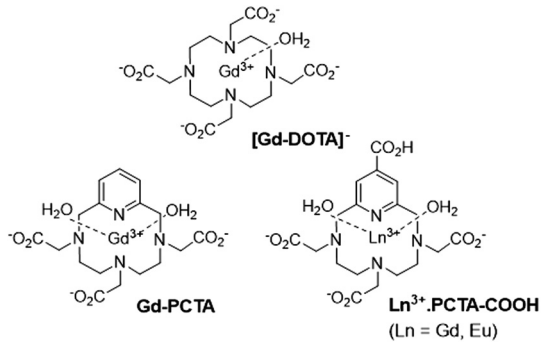

Fig. 1 Structures of the corresponding lanthanide complexes of DOTA, PCTA and PCTA-COOH ligands (see text). Ln^{3+}·PCTA-COOH are new complexes described in this work.

which, due to geometrical contraints, does not participate in the coordination of the Ln^{3+} ion unlike the three pendant acetate arms. The 4-position carboxylic acid function of PCTA-COOH will allow a strong competitive interaction with zirconium ions such as with the double-hydrophilic block copolymer during the formation of the monodisperse nano-objects. Additionally, the pyridine unit of PCTA-COOH is capable of acting as a sensitizer, enhancing the luminescence of Eu(III) ion with a long emission lifetime in the visible region.[31–33] Due to the similar chemical behaviour of Eu(III) and Gd(III) ions, the corresponding Eu(III) chelate of PCTA-COOH ligand is also used to provide a good structural model of Gd^{3+}·PCTA-COOH/Zr@HPICs. Luminescence of the europium ion will lead to complementary information on these HPICs architectures.

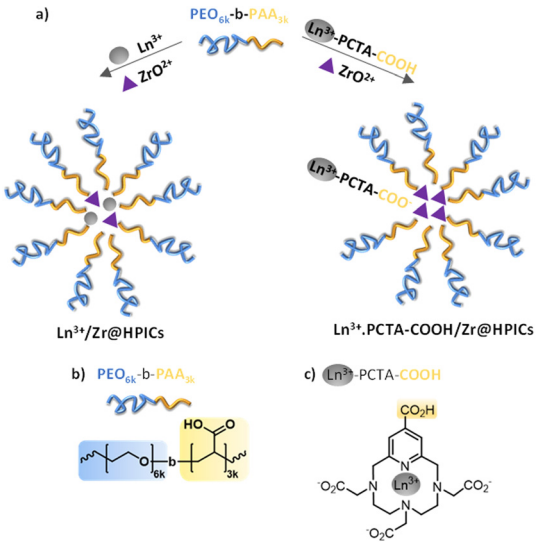

Scheme 1 Schematic representation of the strategy used in this work. (a) The addition of ZrO^{2+} and Ln^{3+} in free form and in the form of Ln^{3+}-PCTA-COOH complexes to the double hydrophilic block copolymer PEO_{6k}-*b*-PAA_{3k} leads to polymeric nanoparticles named Ln^{3+}·PCTA-COOH/Zr@HPICs or Ln^{3+}/Zr@HPICs (Ln = Eu, Gd). (b) Chemical structure of the diblock copolymer used in this work: poly (acrylic acid) and a poly(ethylene oxide) block have average molecular weights of 6000 and 3000 g mol^{-1} respectively. The polymer is noted PEO_{6k}-*b*-PAA_{3k}. (c) Structure of the Ln^{3+}-PCTA-COOH complexes used and described in this work. Carboxylic acid function of the isonicotinic moiety has a pK_a around 1.8.

2. Results and discussion

2.1. Synthesis and characterization of Ln(III) complexes derived from PCTA-COOH

PCTA-COOH ligand was synthetized following an established procedure,[34] in an eight-step with a 50% overall yield using a convergent pathway as shown in ESI Scheme S1.† The lanthanide complexes Ln^{3+}·PCTA-COOH (Ln = Eu, Gd) were obtained by mixing a stoichiometric amount of lanthanide chloride hexahydrate in aqueous solution of PCTA-COOH ligand while maintaining the pH at 5 (Scheme 2).

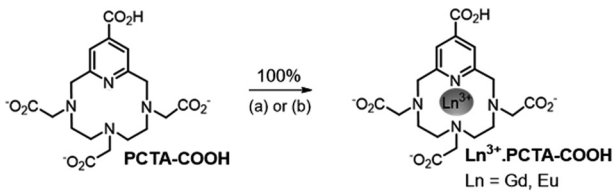

Scheme 2 Synthesis of Eu^{3+} and Gd^{3+} complexes derived from PCTA-COOH. Reagents and conditions: (a) $GdCl_3{\cdot}6H_2O$, H_2O-NaOH, pH 5–6, rt 16 h; (b) $EuCl_3{\cdot}6H_2O$, H_2O-NaOH, pH 5–6, rt 16 h.

After the complexation was completed, the pH was adjusted to 7 with NaOH 1 M. Purification on a C18 chromatography column (1/1: water/methanol) afforded pure complexes characterized by UPLC and high-resolution mass spectrometry (Fig. S1–S4 in ESI†). Identical UPLC retention times for the two complexes confirm the similar chemical properties of the two lanthanide ions complexed. Some UV absorption and time-resolved luminescence properties determined in 0.05 M Tris buffer pH 7.4 at 298 K for the europium complex are gathered in Table 1.

Upon photoexcitation into the ligand absorption band at 281 nm, the Eu^{3+}·PCTA-COOH complex emits characteristic red photoluminescence attributed to the $^5D_0 \rightarrow {}^7F_J$ (J = 0–6) transitions of the europium ion, as shown in Fig. 2. This spectrum is mainly contributed to by the hypersensitive $^5D_0 \rightarrow {}^7F_2$ transition and the $^5D_0 \rightarrow {}^7F_1$, $^5D_0 \rightarrow {}^7F_4$ transitions. The sensitized nature of the europium emission is confirmed by the photoluminescence excitation spectrum, which perfectly overlaps the spectral signature of the antenna pyridine in the UV spectrum of the Eu^{3+}·PCTA-COOH complex. The metal luminescence lifetime of complex at room temperature is 0.39 ms. Upon solvent deuteration, this lifetime increases by a factor of about five, indicating of strong coupling between the metal ion and O–H oscillators of the solvent, which favors radiationless deactivation of the metal excited state.

Using the well-established empirical relation of Horrocks[35] to estimate the apparent hydration state q of the complex, these results indicate the presence of two metal-bound water molecules in the Eu^{3+}·PCTA-COOH complex. This aligns with the expected seven-coordinating-nature of ligand and the preferred coordination number of 8–9 for Eu^{3+}.

2.2. Formation and characterization of HPICs

Zirconyl ions have a high affinity for carboxylic functions[36,37] which have long been used in medical applications without reported adverse effects.[38] Their addition to a solution comprising a mixture of Ln^{3+}·PCTA-COOH and the diblock PEO_{6k}-*b*-PAA_{3k} copolymer induces the formation of HPICs once electroneutrality is reached between the positive charges of ZrO^{2+} ions and the potentially available negative charges from the ionized or ionizable carboxylic acid.[26] This interaction enables, as illustrated in Scheme 1, the incorporation of Ln^{3+}·PCTA-COOH complexes in HPICs architecture which will be named in the following Ln^{3+}·PCTA-COOH/Zr@HPICs. To assess the role of Ln^{3+}·PCTA-COOH, model systems with free Gd^{3+} and Eu^{3+} species were also formed. In this case, a mixture of Gd^{3+} or Eu^{3+} and ZrO^{2+} ions is added to an aqueous solution of the diblock PEO_{6k}-*b*-PAA_{3k} copolymer (0.1 wt%) respecting electroneutrality (see Experimental section). Ln^{3+}/Zr@HPICs complexes are thus obtained. Concerning the respective content of Ln^{3+} and ZrO^{2+}, previous experiments on Gd^{3+}/Zr@HPICs systems have demonstrated that optimal relaxivity properties were obtained for a Gd content equal to 5–10% of the total amount of ions.[26] Therefore a targeted ratio equal to 10% was initially chosen for Ln^{3+}·PCTA-COOH/Zr@HPICs. The amount of lanthanide respective to the total amount of ions was estimated from ICP/MS measurements after purification through a dialysis/centrifugation process and are reported in Table 2.

The molecular weight cut-off of the filter was chosen at 3 kDa, enabling the retention of HPICs structures while free Ln^{3+}·PCTA-COOH complexes are filtered out. It was found that 60% of the introduced Ln^{3+}·PCTA-COOH was retained within the dialysed HPICs, resulting in a final content of 6 ± 1% of Ln^{3+} (Fig. S5 in ESI†). In the case of Ln^{3+}/Zr@HPICs, all introduced Ln^{3+} remained within the final HPICs, and the targeted

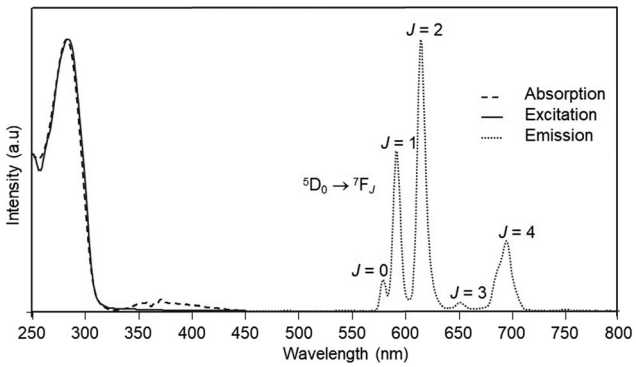

Fig. 2 Normalized absorption, corrected excitation (λ_{em} = 616 nm) and emission spectra (λ_{exc} = 281 nm) of Eu^{3+}·PCTA-COOH in Tris buffer (pH 7.4) at 298 K. The emission bands arise from $^5D_0 \rightarrow {}^7F_J$ transitions; the J values are shown on the spectrum.

Table 1 Key photophysical data (absorption properties, luminescence lifetimes) for Eu^{3+}·PCTA-COOH in 0.05 M Tris buffer pH 7.4 at 298 K

λ_{abs}/nm (ε/M^{-1} cm^{-1})	τ_H [a] (ms)	τ_D [a] (ms)	$q \pm 0.1$ [b]
281 (3600)	0.39	2.18	1.99

[a] Tris buffer prepared in H_2O solution (H) or D_2O (D) solution. [b] Number of coordinated H_2O molecules q calculated using the following equation $q = 1.11[(\tau_H)^{-1} - (\tau_D)^{-1} - 0.31]$.

Table 2 Studied HPICs nano-objects containing either gadolinium or europium (free or as complexes) mixed with zirconium in various mole fractions

HPICs nano-objets	Ln [a] (%)	R_h [b] (nm)	$q \pm 0.1$ [c]	r_1 [d] (mM^{-1} s^{-1})
Eu^{3+}/Zr@HPICs	6	7.7 ± 2.3	4.3	—
Eu^{3+}·PCTA-COOH/Zr@HPICs	5	9.7 ± 4.0	1.9	—
Gd^{3+}/Zr@HPICs	6	9.8 ± 3.0	—	66.5 ± 0.7
Gd^{3+}·PCTA-COOH/ Zr@HPICs	5	10.1 ± 5.9	—	8.0 ± 0.2

[a] Molar amount of lanthanide respective to the total amount of ions estimated from ICP/MS measurements after purification through a dialysis/centrifugation process (±1%). [b] Hydrodynamic radius (and standard deviation) R_h estimated by cumulant analysis of DLS experiments. [c] Number of coordinated H_2O molecules q estimated for Eu systems from luminescence measurements and calculated using the following equation $q = 1.11[(\tau_H)^{-1} - (\tau_D)^{-1} - 0.31]$. [d] Estimated for Gd systems from relaxivity measurements in H_2O (pH 6.8–7) at 298 K.

values for Ln content were chosen to be closed to those of Ln^{3+}·PCTA-COOH/Zr@HPICs (*i.e.* 5%, Table 2).

Obtained colloidal systems were further characterized by DLS measurements (Fig. 3 and Fig. S6†). Well-defined HPICs were formed with a hydrodynamic radius around 10 nm similarly to the size obtained for HPICs based on Cu^{2+}, Fe^{3+}, Ga^{3+} or Gd^{3+} with a similar block copolymer (Table 2).[18,39–41] The number of lanthanide and zirconyl ions within one Ln^{3+}/Zr@HPIC can be roughly estimated from previous studies on Gd@HPICs and Ga@HPICs based on the same polymer and is a around 1000 thousand ions (*i.e.* 50 ions lanthanide per nano-objects).[41]

2.3. Luminescence properties of Eu^{3+}-based HPICs

The study of the luminescence properties of europium-based systems is particularly interesting because these properties are highly sensitive to the europium environment. The encapsulation of Eu^{3+} in macrocyclic complexes or in HPICs structures results in the partial substitution of the nine water molecules surrounding the ion by donor atoms from the polymeric or macrocyclic compound. Consequently, non-radiative deactivations associated with the presence of water molecules that are in a first approximation proportional to the number of molecular oscillators of the O–H type in the ion's first coordination sphere are minimized.[42] This results in enhanced luminescence properties in the studied complexes compared to free Eu^{3+} ions. Emission spectra (λ_{ex} = 287 nm) of the different studied systems are shown in Fig. 4. In the case of Eu^{3+}·PCTA-COOH/Zr@HPICs, as for Eu^{3+}·PCTA-COOH free complex, where the pyridine unit of PCTA-COOH acts as an "antenna", a strong red emission was detected at 590 nm and 615 nm, corresponding respectively to the $^7D_0 \rightarrow {}^7F_1$ and $^7D_0 \rightarrow {}^7F_2$ transitions of Eu^{3+},[43] while no transition was detected in the emission spectrum of an aqueous solution of $Eu(NO_3)_3$ with a similar concentration of Eu^{3+} (0.12 mM).

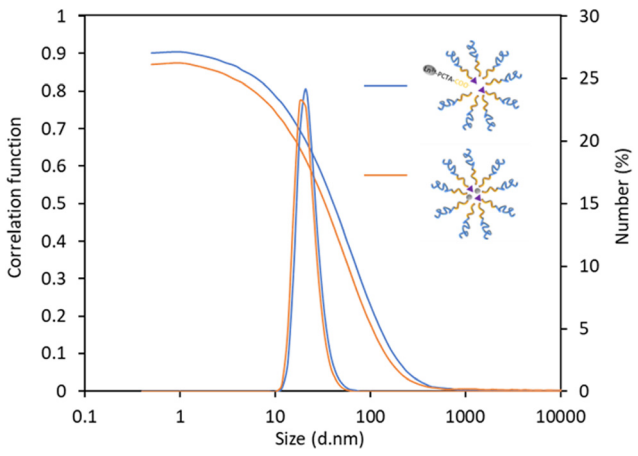

Fig. 3 Number-averaged hydrodynamic diameter distribution obtained on Eu^{3+}/Zr@HPICs (orange) and Eu^{3+}·PCTA-COOH/Zr@HPICs (blue) from DLS measurements (polymer concentration equal to 0.1 wt%) at pH 7 and corresponding NNLS analysis. Correlation functions from which these distributions are issued are superimposed on these distributions and clearly demonstrate the absence of aggregates in studied solutions (NB: for these correlation functions *X*-axis values corresponding to correlation time is not given, see Fig. S6†).

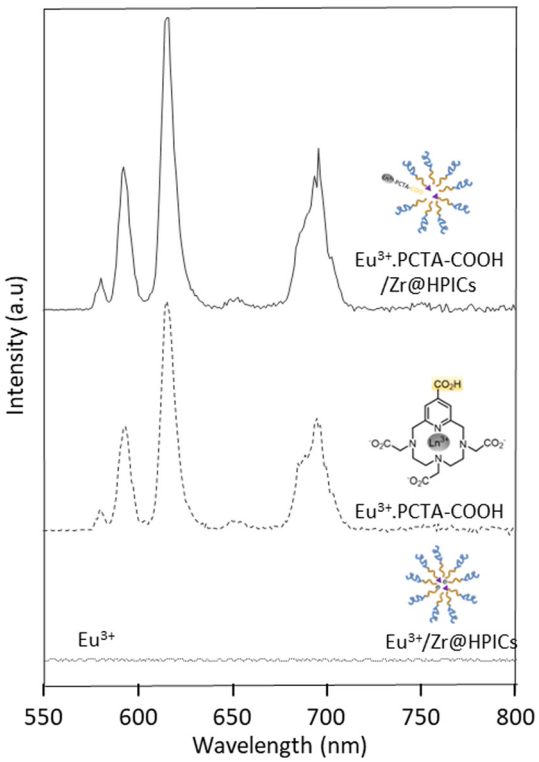

Fig. 4 Corrected emission spectra (λ_{exc} = 287 nm) of Eu^{3+}, Eu^{3+}/Zr@HPICs, Eu^{3+}·PCTA-COOH and Eu^{3+}·PCTA-COOH/Zr@HPICs in H_2O (pH 6.8–7) at 298 K ([Eu] = 0.12 mM).

Moreover, the number of water molecules in the first coordination sphere of Eu^{3+} ions, estimated using luminescence lifetime measurements, was found to be around 1.9 ± 0.1 water molecules, which is similar to that of Eu^{3+}·PCTA-COOH complex (*i.e.* 1.99, Table 1). The insertion of Eu^{3+}·PCTA-COOH within HPICs did not affect its luminescence properties and did not lead to a decomplexation phenomenon induced by the presence of carboxylic function of the polymer. As expected, for a similar concentration of Eu^{3+}, the luminescence measured for Eu^{3+}/Zr@HPICs is barely visible (Fig. 4). Indeed, for this system, the number of water molecules in the first coordination sphere of Eu^{3+} ions, estimated using luminescence lifetime measurements, was found to be at a significant higher value,[44] around 4.3 ± 0.1. Additionally, no antenna effect can promote luminescence properties. In view of the use of Gd^{3+}·PCTA-COOH/Zr@HPICs as contrast agents, particular attention must be paid to the maintenance of their integrity in the presence of competing ions at physiological pH, due to the high toxicity of the free gadolinium ion. In this context, measurements of luminescence intensities and lifetimes were performed on europium-based analogues in 50 mM Tris buffered saline pH 7.4 ([NaCl] = 0.15 M) and after addition of phosphate ions or calcium ions (Fig. 5A). The luminescence

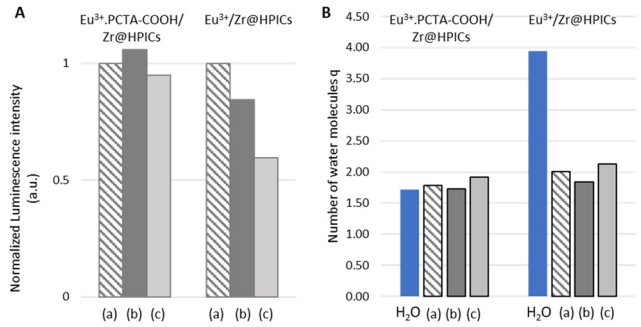

Fig. 5 Effects of added ions on Eu^{3+}·PCTA-COOH/Zr@HPICs and Eu^{3+}/Zr@HPICs ([Eu] = 0.12 mM). (A) Normalized luminescence intensity (area-normalized emission spectra, λ_{exc} = 287 nm) (a) in Tris buffered saline 50 mM pH 7.4 ([NaCl] = 0.15 M), and after adding (b) phosphate (0.10 mM) and (c) calcium ions (0.25 mM). (B) Number of coordinated H_2O molecules q estimated for Eu systems from luminescence lifetime measurements and calculated using the following equation $q = 1.05 \times 1/\tau_H - 0.70$, in H_2O at pH 6.8–7, (a) in Tris buffered saline 50 mM pH 7.4 ([NaCl] = 0.15 M), and after adding (b) phosphate (0.10 mM) and (c) calcium ions (0.25 mM).

intensities and lifetimes of the Eu^{3+}·PCTA-COOH/Zr@HPICs system measured in pure water are not modified in Tris buffer, as well as after the addition of phosphate ions or calcium ions. The hydration parameter q = 2 remains unchanged (Fig. 5B). These observations are thus indicative of good integrity of the entity in the physiological media studied. For the Eu^{3+}/Zr@HPICs system, several parameters are affected. On the one hand, compared to pure water, a significant decrease of the hydration parameter q is observed for the entity in solution in Tris buffer (Fig. 5B). This indicates an interaction between the Eu^{3+} ion and the Tris buffer (2-amino-2-(hydroxymethyl) propane-1,3-diol), probably *via* the amino group,[45,46] which induces the partial replacement of 2 of the 4 coordinated water molecules. On the other hand, in Tris buffer, the luminescence intensities of Eu^{3+}/Zr@HPICs are decreased by 20% and 40%, respectively, after the addition of phosphate and calcium ions (Fig. 5A), without affecting the luminescence lifetimes (Fig. S7†). This result highlights a partial release of Eu^{3+} ions under these conditions and thus indicates a lower stability of the Eu^{3+}/Zr@HPICs entity in the physiological media studied.

The stability of europium ions as a function of pH was further studied (Fig. S8†). While the Eu^{3+}@HPICs structure shows a decrease of more than 80% in measured intensity as the pH value increases, the insertion of zyrconyl ions into the Eu^{3+}/Zr@HPICs structure prevents this phenomenon to a large extent. However, to maintain both luminescence properties and the coordination sphere of europium ions, its insertion through PCTA complexes remains the solution of choice.

2.4. Relaxivity properties of Gd^{3+}-based HPICs

The relaxivity of Gd^{3+}/Zr@HPICs and Gd^{3+}·PCTA-COOH/Zr@HPICs was further studied in aqueous medium at physiological pH (Fig. S9 in ESI†). In water, the r_1 relaxivity values of Gd^{3+}/Zr@HPICs, Gd^{3+}·PCTA-COOH/Zr@HPICs, and Gd^{3+}·PCTA-COOH were measured to be 66.5 ± 0.7 mM^{-1} s^{-1}, 8.0 ± 0.2 mM^{-1} s^{-1} and 2.8 ± 0.3 mM^{-1} s^{-1}, respectively (25 °C, 0.47 T). The inclusion of the complexes in the HPICs structure induces, as expected, an increase in the measured relaxivity by a factor of three. However, this relaxivity remains significantly lower than that of the Gd/Zr@HPICs. In the latter case, this efficiency might be ascribed to more efficient water diffusion within the polymer matrix.[26] The values measured in the case of macrocyclic complexes encapsulated in HPICs fall within ranges comparable to those measured for gadolinium-based inorganic particles, such as $GdPO_4$ and $NaGdF_4$. For these inorganic systems, relaxivity values between 1 and 30 mM^{-1} s^{-1} have been measured, depending on the particle size and the nature of the stabilizing agent used.[3] Moreover, these values surpass those measured for commercial molecular complexes which are lower than 6 mM^{-1} s^{-1} in human plasma at 37 °C and 0.47 T.[47] When mixed with Tris buffered saline (pH 7.4, 50 mM), the relaxivity remains roughly constant for Gd^{3+}·PCTA-COOH and Gd^{3+}·PCTA-COOH/Zr@HPICs, with measured values at 3.30 ± 0.5 mM^{-1} s^{-1} and 6.0 ± 2.0 mM^{-1} s^{-1}, respectively. Nevertheless, a significant decrease was measured for Gd^{3+}/Zr@HPICs at 23.1 ± 1.0 mM^{-1} s^{-1}, in agreement with the observed decrease on the hydration parameter q from 4 to 2, as measured by luminescence for the analog Eu/Zr@HPICs in Tris buffered saline medium. As previously described,[26] HPICs based on PEG-PAA present an insignificant cytotoxicity up to 1.3 mM Gd (0.1 wt% of polymer). This enables to perform *in vivo* experiments on mice and to obtain preliminary determinations of MR contrast efficacy, pharmacokinetic properties, and tolerance.

2.5. *In vivo* experiments

In vivo MRI contrast was assessed after an intravenous (IV) bolus injection of Gd^{3+}/Zr@HPICs and Gd^{3+}·PCTA-COOH/Zr@HPICs, and it was compared to Gd^{3+}·PCTA-COOH at an equivalent Gd concentration. Tissue uptake and elimination characteristics were analyzed using a T_1-weighted dynamic sequence of coronal images centered on the abdominal cavity. Images were taken for 60 minutes post-IV injection at a dose of 15 μmol kg^{-1} equivalent Gd concentration, with a control image captured at 24 hours. Signal intensities from the regions of interest *i.e.*, vascular (inferior aorta), renal medulla, and bladder spaces were quantified (see Fig. 6). As anticipated, a rapid increase in signal intensity in the vascular space was observed following the injection. At the 30-minute mark, the contrast enhancements for Gd^{3+}/Zr@HPICs, Gd^{3+}·PCTA-COOH/Zr@HPICs and Gd^{3+}·PCTA-COOH were significantly different, registering at 41%, 20%, and 15%, respectively. Monitoring of bladder signal intensity enables the assessment of urinary excretion of the compounds. The intensities measured for the three compounds differ significantly. Gd^{3+}·PCTA-COOH and, to a lesser extent, Gd^{3+}·PCTA-COOH/Zr@HPICs induce contrast enhancement in urine, whereas Gd^{3+}/Zr@HPICs does not (Fig. 6 – bladder).

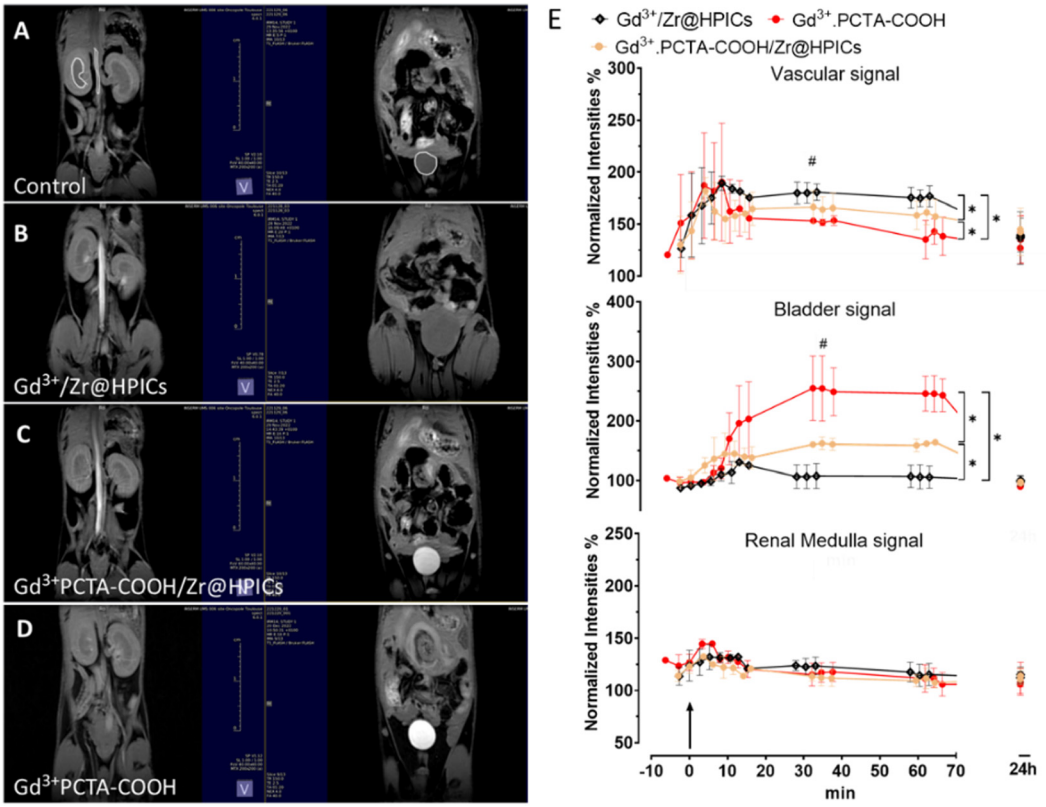

Fig. 6 Dynamics of signal intensities in mouse tissues following administration of Gd^{3+} complex agents. Typical images of horizontal abdominal sections at the level of the kidneys and lower aorta (left) and the bladder (right) are shown: (A), pre-injection control – regions of interest for the renal medulla, vascular space, and bladder are delineated in white; (B–D) 60 min post-intravenous injection of Gd^{3+}/Zr@HPICs, Gd^{3+}·PCTA-COOH/Zr@HPICs and Gd^{3+}·PCTA-COOH respectively; (E) evolution of normalized intensities for the vascular space, bladder, and renal medulla is depicted (black arrow indicates the time of injection). Significant differences between the mean normalized intensities (# and *) were observed ($p < 0.01$, $n = 3$) 30 min and 60 min post-administration, respectively ([Gd^{3+}] = 0.12 mM).

While Gd^{3+}·PCTA-COOH behaved similarly to DOTAREM,[24] characterized by rapid excretion in tandem with the decline in vascular space signal intensity, Gd^{3+}/Zr@HPICs shows a behavior similar to the one observed for HPICs based on the complexation of double hydrophilic block copolymers comprising an outer PEG shell, as previously described in the literature.[18,19,23] Gd^{3+}·PCTA-COOH/Zr@HPICs shows an intermediate behavior. The evolution of the signal suggests that some of the complexes encapsulated in the HPICs structure are rapidly released and contribute to the observed signal enhancement in the bladder, while those interacting more strongly remain in the HPICs structure and extend the lifetime of the signal in the various organs. None of the administered compounds caused alterations in the renal medullary signal in these healthy animals.

3. Experimental section/methods

3.1. Materials

$Gd(NO_3)_3{\cdot}6H_2O$, $GdCl_3{\cdot}6H_2O$, $ZrOCl_2{\cdot}8H_2O$, $Eu(NO_3)_3{\cdot}5H_2O$, $EuCl_3{\cdot}6H_2O$ and $Ga(NO_3)_2{\cdot}6H_2O$ were purchased from Sigma Aldrich Co., Ltd. At highest purity available and used as received. PEO_{6k}-*b*-PAA_{3k} was purchased from Polymer Source™ and used as received. Water was purified through a filter and ion exchange resin using a Purite device (resistivity 18.2 MΩ cm). D_2O was obtained from Eurisotop.

3.2. Synthesis

Synthesis of Eu^{3+} and Gd^{3+} complexes: Eu^{3+}·PCTA-COOH and Gd^{3+}·PCTA-COOH. To a solution of ligand PCTA-COOH[34] in H_2O was added $EuCl_3{\cdot}6H_2O$ or $GdCl_3{\cdot}6H_2O$ (1.1 equiv.). After stirring at room temperature for 1 h, pH was adjusted to 5–6 with NaOH 0.1 M and the mixture was then stirred for 16 h at room temperature. The pH was then adjusted to 7 with NaOH 0.1 M, the solvent was evaporated to a minimum and the solution was loaded on a Waters Sep-Pak® cartridge (C18, 10 g). Cartridge was rinsed with H_2O to remove salts and the product was eluted with a H_2O/MeOH 1 : 1 mixture. The solvents were removed *in vacuo* to give the expected complex with quantitative yield. The absence of free lanthanide ions was verified using a classic test with an arsenazo indicator solution.

Eu^{3+}·PCTA-COOH complex. UPLC analysis: t_R = 4.11 min. HRMS (ESI positive ion mode): *m*/*z* calcd for $C_{18}H_{22}N_4O_8{}^{151}Eu$ $[M + H]^+$ 573.0636, found 573.0643 (Δm = 1.2 ppm). UV λ_{abs}

(Tris buffer, pH 7.4)/nm 281 (ε = 3600 M^{-1} cm^{-1}). Fluorescence λ_{em} (Tris buffer, pH 7.4, λ_{exc} = 281 nm)/nm 580 (relative intensity, corrected spectrum 2.4), 592 (17.8), 615 (41.7), 651 (2.2), 695 (35.9).

Gd^{3+}·PCTA-COOH complex. UPLC analysis: t_R = 4.25 min. HRMS (ESI positive ion mode): *m*/*z* calcd for $C_{18}H_{22}N_4O_8{}^{156}Gd$ $[M + H]^+$ 578.0663, found 578.0670 (Δm = 1.2 ppm). UV λ_{abs} (Tris buffer, pH 7.4)/nm 282 (ε = 3900 M^{-1} cm^{-1}).

Gd^{3+}·PCTA-COOH/Zr@HPICs and Eu^{3+}·PCTA-COOH/Zr@HPICs formation. The formation of Ln^{3+}·PCTA-COOH/Zr@HPICs was obtained by adding a solution of zirconyl ions to a solution comprising a mixture of Ln^{3+}·PCTA-COOH and diblock PEO_{6k}-*b*-PAA_{3k} copolymer. The ratio of charge between the positive charges due to the zirconyl ZrO^{2+} ions and the negative ones due to carboxylic functions (coming either from acrylic acid polymer units or from the free carboxylic function of PCTA-COOH) was chosen equal to one. In addition, the molar fraction of lanthanide ions was chosen equal to 10% relatively to the total amount of lanthanide and zirconyl ions. After purification through a dialysis/centrifugation process, this fraction estimated from ICP/MS measurements was found equal to 6 ± 1%. Therefore, the final concentrations of acrylic acid unit, zirconyl ions and lanthanide ions *i.e.* Ln^{3+}·PCTA-COOH complexes are equal to 2.68 × 10^{-3} mol L^{-1}, 1.40 × 10^{-3} mol L^{-1} and 0.12 × 10^{-3} mol L^{-1} respectively.

Gd^{3+}/Zr@HPICs and Eu^{3+}/Zr@HPICs formation. Solutions of HPICs were formed by mixing an aqueous solution of PEO_{6k}-*b*-PAA_{3k} with a solution containing $Gd(NO_3)_3{\cdot}6H_2O$ or $Eu(NO_3)_3{\cdot}5H_2O$ and $ZrOCl_2{\cdot}8H_2O$. Gadolinium or europium and zirconium concentrations were adjusted in order to have a molar fraction of gadolinium or europium to zirconyl ions equal to 5% within the HPICs (to have roughly the same value than the one obtained for Ln^{3+}·PCTA-COOH/Zr@HPICs, *i.e.* 5–6%). The ratio of charge between the charges due to the metallic ions and that due to the polymers was set to be close to unity for all experiments. After mixing, the pH of the solutions was adjusted to 6.8–7. In that case, after purification through a dialysis/centrifugation process, the final concentrations of acrylic acid unit, zirconyl ions and lanthanide ions are equal to 2.68 × 10^{-3} mol L^{-1}, 1.16 × 10^{-3} mol L^{-1} and 0.12 × 10^{-3} mol L^{-1} respectively.

3.3. Methods

Characterization of Ln^{3+}·PCTA-COOH (Ln = Eu^{3+}, Gd^{3+}). ^1H NMR spectra were recorded using a Bruker Avance 300 spectrometer with D_2O as solvent. Chemical shifts δ are reported in parts per million (ppm) and are referenced to the residual solvent peak (D_2O : H = 4.79 ppm).

High-Resolution Mass Spectra (HRMS) were obtained on a Xevo G2 Qtof Waters spectrometer. The UPLC analyses were performed on a Waters UPLC Acquity apparatus with PDA (photodiode array) and SQ (simple quadripole) detectors, and using an Acquity BEH HILIC column (1.7 μm, 100 × 2.1 mm) with a flow rate of 0.4 mL min^{-1}. Linear gradient system was H_2O + 0.1% HCOOH (pH 2)/CH_3CN + 0.1% HCOOH (pH 2) 5/95 to 50/50 in 7 min, then an isocratic elution 50/50 for 10 min. Absorption measurements were done with a Hewlett Packard 8453 temperature-controlled spectrometer in 10 mm quartz cuvette.

Emission, excitation spectra and luminescence decays of europium complex were measured using a Cary Eclipse spectro fluorimeter equipped with a Xenon flash lamp source and a Hamamatsu R928 photomultiplier. Excitation spectra were corrected for the excitation light intensity, while emission spectra were corrected for the instrument response. Lifetimes τ (uncertainty ≤ 5%) are made by monitoring the decay at 616 nm, a wavelength corresponding to the maximum intensity of the emission spectrum, following pulsed excitation. They are the average values from at least five separate measurements covering two or more lifetimes. The luminescence decay curves were fitted by an equation of the form $I(t) = I(0)\exp(-t/\tau)$ by using a curve-fitting program. The average number of coordinated water molecules on europium ions in complex (free or in HPICs) were determined as follow: solutions of PEO_{6k}-*b*-PAA_{3k} polymers (0.1 wt%) with various amounts of Eu^{3+} and ZrO^{2+} were prepared to get HPICs solutions with ρ_{charge} = 1 and ρ_{Eu} equal to 5%. After adjusting of the pH of the solutions to *ca.* 6.8–7, luminescence of the solutions was measured. The solutions were freeze-dried the redispersed in D_2O with final concentrations equivalent to that in water. DLS experiments on such redispersed solution suggest that the HPICs are maintained during this process. Luminescence of the D_2O solutions was then recorded. Using the equation proposed by R.M. Supkowski *et al.*,[35] the number (q) of water molecules coordinated to the europium ions within the HPICs was estimated.[48]

Characterization of Ln^{3+}/Zr@HPICs and Ln^{3+}·PCTA-COOH/Zr@HPICs (Ln = Eu^{3+}, Gd^{3+}) properties

Colloidal stability. Dynamic light scattering measurements were conducted using a Zetasizer Nano-ZS (Malvern Instruments, Ltd, UK) with an integrated 4 mW He–Ne laser, λ = 633 nm. Light scattering intensity (at 173°) was measured with instrumental parameters set to constant values for all the samples. The correlation function was analyzed *via* the cumulant method to get the *Z*-average size of the colloids and by the general-purpose method (NNLS) to obtain their distribution in size. The apparent equivalent hydrodynamic radius R_h were then determined using the Stokes–Einstein equation $D = (k_BT)/(6\pi\eta R_h)$ where T is the temperature and η the viscosity of the solution. Mean radius values were obtained from five different runs of the number plot.

Composition. Inductively coupled plasma – atomic emission spectroscopy (ICP-AES) analysis was performed by Antellis company (**https://www.antellis.com**). Measurements were performed on an ULTIMA 2 inductively coupled plasma atomic emission spectrometer from Horiba Jobin Yvon Technology. To enable analyses, a specific nebulizer (PTFE Mira Mist Nebulizer, supplied by Horiba Jobin Yvon Technology) was used to introduce the solution into the ICP-AES. The nebulizer was inserted into a glass cyclonic chamber and operated at a maximum sample flow rate of 1 ml min^{-1} and with a maximum total dissolved solute of 300 g L^{-1}. The optical wave-

length for each element was determined to optimize the limits of quantification through calibration curves with 0–10 ppm concentrations (5 points). The sample was introduced into the ICP-AES instrument with a peristaltic pump.

Relaxivity. Magnetic relaxation time measurements in solution were carried out at 1.4 T on a Minispec mq60 TD-NMR contrast agent analyser (Bruker Optics, Billerica, MA, USA) at a constant temperature of 25 °C. T_1 relaxation times were measured using an inversion recovery pulse sequence; T_2 relaxation times were measured using a Carr–Purcell–Meiboom–Gill pulse sequence. Experiments were performed on solutions with 0.1 wt% of polymers.

3.4. *In vivo* experiments

Nine BALB/cOlaHsd mice (Envigo) aged 10–12 weeks were used for MRI experiments. All *in vivo* experimental procedures were approved by our institutional animal care and use committee CEEA122 (APAFIS 5192-2016041911336422 and 34703-2022011811542488) and conducted in compliance with the Ethics Committee pursuant to European legislation translated into French Law as Decret 2013-118 dated 1st of February 2013.

Small animal MRI. Animals were anesthetized with isoflurane (induction 3%–4%, maintenance 1.5% (isoflurane/O_2)) to insert a catheter in the tail vein. Then, the mice is placed in a specific MRI imaging cell (Minerve, Esternay, France) to preserve the health status (SPF), ensure the temperature regulation and the breathing monitoring. Animals received a dose of 15 μmol kg^{-1} of Gd equivalent followed by a 200 μl flush of saline. MR image acquisitions were performed on a Biospec 7T dedicated to small animals (Bruker, Wissenbourg, France). Acquisitions of the abdominal images were carried out with a 40 mm transmit-receive volume coil and triggered on breathing to reduce motion artifacts. T_1 weighted images were acquired using Flash sequence with the following parameters: TR = 150 ms; TE = 2.5 ms; flip angle: 40°; number of average: 4; FOV: 40 × 40 mm; resolution 200 × 200 μm; 13 slices of 1 mm thickness; fat suppression; acquisition time: 1 min 20 s. Intensity values were normalized against muscle intensity and given in percentage. Mean Intensity data are shown as mean ± SD (n = 3 per contrast agent). An unpaired t-test was used to assess differences between normalized intensities recorded at 30 min ± 5 min and 60 ± 5 min (3 values per contrast agent). A p-value less than 0.01 was considered significant.

4. Conclusions

Lanthanide-based macrocycles Ln^{3+}·PCTA-COOH are successfully inserted in hybrid polyionic complexes colloidal structures thanks to the interaction of the 4-position carboxylic acid function of PCTA-COOH with zirconium ions during the formation of the monodisperse nano-objects. These obtained nanoobjects, with an average radius of *ca.* 10–15 nm, present good colloidal and chemical stability in physiological medium. Moreover, the lanthanide incorporated as Ln^{3+}·PCTA-COOH complex in HPICs avoid the partial release of lanthanide ions even in the presence a significant excess of phosphate or calcium ions, endogenous ions potentially interacting with lanthanide ions. Preliminary determinations of MRI contrast efficacy, pharmacokinetic and optical properties and tolerance performed *in vivo* in mice show that these colloids including Ln^{3+}·PCTA-COOH complexes benefit from both their colloidal nature and the specific properties of the lanthanide complexes: while they retain the optical properties and chemical stability of initial Ln^{3+}·PCTA-COOH complexes, the magnetic properties and *in vivo* distribution benefit from the colloidal nature of the nanoobjects formed. Therefore, the strategy proposed in this article opens up new opportunities to pave the way for new applications for metal complexes based on the use of cryptants, whether in biology or catalysis.

Conflicts of interest

There are no conflicts to declare.

Acknowledgements

The authors thank the "Agence National pour la Recherche" for funding (ANR Hybrid MRI, no ANR-19-CE09-0011-01) as well as the financial support of Toulouse Tech transfer and Region Occitanie (FESR_PREMAT-000025/prématuration 2017 Hybrid-MRI). The authors wish to thank Charles-Louis Serpentini and Stéphane Gineste for the help with fluorimetry and DLS experiments respectively (Softmat, Toulouse, France) and CREFRE-Oncopole Experimental zootechny team (Inserm CREFRE-Anexplo, Toulouse France) for animal housing.

References

1 G. K. Das, B. C. Heng, S.-C. Ng, T. White, J. S. C. Loo, L. D'Silva, P. Padmanabhan, K. K. Bhakoo, S. T. Selvan and T. T. Y. Tan, *Langmuir*, 2010, **26**, 8959.
2 M. A. Sieber, P. Lengsfeld, J. Walter, H. Schirmer, T. Frenzel, F. Siegmund, H.-J. Weinmann and H. Pietsch, *J. Magn. Reson. Imaging*, 2008, **27**, 955.
3 M. Yon, C. Billotey and J.-D. Marty, *Int. J. Pharm.*, 2019, **569**, 118577.
4 E. S. Harpur, D. Worah, P.-A. Hals, E. Holtz, K. Furuhama and H. Nomura, *Invest. Radiol.*, 1993, **28**, S28.
5 A. Radbruch, L. D. Weberling, P. J. Kieslich, O. Eidel, S. Burth, P. Kickingereder, S. Heiland, W. Wick, H.-P. Schlemmer and M. Bendszus, *Radiology*, 2015, **275**, 783.
6 U. Schmiedl, M. E. Moseley, M. D. Ogan, W. M. Chew and R. C. Brasch, *J. Comput. Assist. Tomogr.*, 1987, **11**, 306.
7 L. Johansson, M. A. Kirchin and H. Ahlström, *Acta Radiol.*, 2012, **53**, 1112.
8 N. Murata, K. Murata, L. F. Gonzalez-Cuyar and K. R. Maravilla, *Magn. Reson. Imaging*, 2016, **34**, 1359.

9 T. Kanda, K. Ishii, H. Kawaguchi, K. Kitajima and D. Takenaka, *Radiology*, 2014, **270**, 834.
10 T. Kanda, M. Osawa, H. Oba, K. Toyoda, J. Kotoku, T. Haruyama, K. Takeshita and S. Furui, *Radiology*, 2015, **275**, 803.
11 P. Caravan, C. T. Farrar, L. Frullano and R. Uppal, *Contrast Media Mol. Imaging*, 2009, **4**, 89.
12 A. J. L. Villaraza, A. Bumb and M. W. Brechbiel, *Chem. Rev.*, 2010, **110**, 2921.
13 Y. Li, S. Laurent, L. Esser, L. V. Elst, R. N. Muller, A. B. Lowe, C. Boyer and T. P. Davis, *Polym. Chem.*, 2014, **5**, 2592.
14 M. Younis, V. Darcos, C. Paniagua, P. Ronjat, L. Lemaire, B. Nottelet, X. Garric, Y. Bakkour, J. H. El Nakat and J. Coudane, *RSC Adv.*, 2016, **6**, 5754.
15 J. Wang, A. H. Velders, E. Gianolio, S. Aime, F. J. Vergeldt, H. Van As, Y. Yan, M. Drechsler, A. de Keizer, M. A. Cohen Stuart, *et al.*, *Chem. Commun.*, 2013, **49**, 3736.
16 J. Wang, R. H. M. De Kool and A. H. Velders, *Langmuir*, 2015, **31**, 12251.
17 F. Cao, T. Huang, Y. Wang, F. Liu, L. Chen, J. Ling and J. Sun, *Polym. Chem.*, 2015, **6**, 7949.
18 C. Frangville, Y. Li, C. Billotey, D. R. Talham, J. Taleb, P. Roux, J.-D. Marty and C. Mingotaud, *Nano Lett.*, 2016, **16**, 4069.
19 K. H. Markiewicz, L. Marmuse, M. Mounsamy, C. Billotey, M. Destarac, C. Mingotaud and J.-D. Marty, *ACS Macro Lett.*, 2022, **11**, 1319.
20 M. Odnoroh, O. Coutelier, C. Mingotaud, M. Destarac and J.-D. Marty, *J. Colloid Interface Sci.*, 2023, **649**, 655.
21 S. Gineste and C. Mingotaud, *Adv. Colloid Interface Sci.*, 2023, **311**, 102808.
22 A. Nabiyan, J. B. Max and F. H. Schacher, *Chem. Soc. Rev.*, 2022, **51**, 995.
23 M. Yon, L. Gibot, S. Gineste, P. Laborie, C. Bijani, C. Mingotaud, O. Coutelier, F. Desmoulin, C. Pestourie, M. Destarac, *et al.*, *Nanoscale*, 2023, **15**, 3893.
24 L. Peng, S. Gineste, C. Coudret, D. Ciuculescu-Pradines, F. Benoît-Marquié, C. Mingotaud and J.-D. Marty, *J. Colloid Interface Sci.*, 2023, **649**, 900.
25 D. B. N. Lee, M. Roberts, C. G. Bluchel and R. A. Odell, *ASAIO J.*, 2010, **56**, 550.
26 M. Yon, S. Gineste, G. Parigi, B. Lonetti, L. Gibot, D. R. Talham, J.-D. Marty and C. Mingotaud, *ACS Appl. Nano Mater.*, 2021, **4**, 4974.
27 G. Tircsó, Z. Kovács and A. D. Sherry, *Inorg. Chem.*, 2006, **45**, 9269.
28 W. D. Kim, G. E. Kiefer, F. Maton, K. McMillan, R. N. Muller and A. D. Sherry, *Inorg. Chem.*, 1995, **34**, 2233.
29 S. Aime, M. Botta, S. G. Crich, G. Giovenzana, R. Pagliarin, M. Sisti and E. Terreno, *Magn. Reson. Chem.*, 1998, **36**, S200.
30 M. Port, I. Raynal, L. Vander Elst, R. N. Muller, F. Dioury, C. Ferroud and A. Guy, *Contrast Media Mol. Imaging*, 2006, **1**, 121.
31 J.-M. Siaugue, F. Segat-Dioury, A. Favre-Réguillon, V. Wintgens, C. Madic, J. Foos and A. Guy, *J. Photochem. Photobiol., A*, 2003, **156**, 23.
32 S. Laurent, L. Vander Elst, C. Galaup, N. Leygue, S. Boutry, C. Picard and R. N. Muller, *Contrast Media Mol. Imaging*, 2014, **9**, 300.
33 G. Bechara, N. Leygue, C. Galaup, B. Mestre-Voegtlé and C. Picard, *Tetrahedron*, 2010, **66**, 8594.
34 N. Leygue, M. Enel, A. Diallo, B. Mestre-Voegtlé, C. Galaup and C. Picard, *Eur. J. Org. Chem.*, 2019, **2019**, 2899.
35 R. M. Supkowski and W. DeW. Horrocks, *Inorg. Chim. Acta*, 2002, **340**, 44.
36 M. Puchberger, F. R. Kogler, M. Jupa, S. Gross, H. Fric, G. Kickelbick and U. Schubert, *Eur. J. Inorg. Chem.*, 2006, **2006**, 3283.
37 U. Schubert, *Chem. Mater.*, 2001, **13**, 3487.
38 D. B. N. Lee, M. Roberts, C. G. Bluchel and R. A. Odell, *ASAIO J.*, 2010, **56**, 550.
39 L. Peng, C. Mingotaud, F. Benoît-Marquié and J.-D. Marty, *ACS Appl. Nano Mater.*, 2022, **5**, 11458.
40 M. Mestivier, J. R. Li, A. Camy, C. Frangville, C. Mingotaud, F. Benoît-Marquié and J. Marty, *Chem. – Eur. J.*, 2020, **26**, 14152.
41 S. Gineste, B. Lonetti, M. Yon, J. Giermanska, E. Di Cola, M. Sztucki, Y. Coppel, A.-F. Mingotaud, J.-P. Chapel, J.-D. Marty, *et al.*, *J. Colloid Interface Sci.*, 2022, **609**, 698.
42 W. D. Horrocks and D. R. Sudnick, *Acc. Chem. Res.*, 1981, **14**(12), 384.
43 K. Binnemans, *Coord. Chem. Rev.*, 2015, **295**, 1.
44 J. Zhang, Y. Liu, Y. Li, H. Zhao and X. Wan, *Angew. Chem.*, 2012, **124**, 4676.
45 J. Pfefferlé and J. G. Bünzli, *Helv. Chim. Acta*, 1989, **72**, 1487.
46 P. Mandal, J. Kretzschmar and B. Drobot, *J. Biol. Inorg. Chem.*, 2022, **27**, 249.
47 M. Rohrer, H. Bauer, J. Mintorovitch, M. Requardt and H.-J. Weinmann, *Invest. Radiol.*, 2005, **40**, 715.
48 P. P. Barthelemy and G. R. Choppin, *Inorg. Chem.*, 1989, **28**, 3354.